

A computational study of discrete mechanical tissue models

To cite this article: P Pathmanathan *et al* 2009 *Phys. Biol.* **6** 036001

View the [article online](#) for updates and enhancements.

You may also like

- [Mechanical characterization of bioprinted *in vitro* soft tissue models](#)

Ting Zhang, Karen Chang Yan, Liliang Ouyang et al.

- [Incorporating cross-voxel exchange into the analysis of dynamic contrast-enhanced imaging data: theory, simulations and experimental results](#)

Noha Sinno, Edward Taylor, Michael Milosevic et al.

- [On the biological basis for competing macroscopic dose descriptors for kilovoltage dosimetry: cellular dosimetry for brachytherapy and diagnostic radiology](#)

R M Thomson, Å Carlsson Tedgren and J F Williamson

physicsworld

AI in medical physics week

20–24 June 2022

Join live presentations from leading experts in the field of AI in medical physics.

physicsworld.com/medical-physics

A computational study of discrete mechanical tissue models

P Pathmanathan¹, J Cooper¹, A Fletcher², G Mirams³, P Murray²,
J Osborne¹, J Pitt-Francis¹, A Walter³ and S J Chapman²

¹ Computing Laboratory, University of Oxford, Wolfson Building, Parks Road, Oxford OX1 3QD, UK

² Mathematical Institute, University of Oxford, 24–29 St Giles’, Oxford, OX1 3LB, UK

³ School of Mathematical Sciences, University of Nottingham, Nottingham, NG7 2RD, UK

E-mail: pras@comlab.ox.ac.uk

Received 29 September 2008

Accepted for publication 16 March 2009

Published 15 April 2009

Online at stacks.iop.org/PhysBio/6/036001

Abstract

A computational study of discrete ‘cell-centre’ approaches to modelling the evolution of a collection of cells is undertaken. The study focuses on the mechanical aspects of the tissue, in order to separate the passive mechanical response of the model from active effects such as cell-growth and cell division. Issues which arise when implementing these models are described, and a series of numerical mechanical experiments is performed. It is shown that discrete tissues modelled this way typically exhibit elastic–plastic behaviour under slow compression, and act as a brittle linear elastic solid under slow tension. Both overlapping spheres and Voronoi–tessellation-based models are examined, and the effect of different cell–cell interaction force laws on the bulk mechanical properties of the tissue is determined. This correspondence allows parameters in the cell-based model to be chosen to be compatible with bulk tissue measurements.

1. Introduction

There are several classes of discrete model of the mechanical behaviour of tissue. The most simple are lattice-based or cellular-automaton models, where cells are constrained to lie on a regular grid (see, for example [1–3]). In such models, each lattice location can contain at most a single cell, possibly drawn from a variety of different cell types, and rules are set up for determining how cells interact, divide and move. Such models do not treat the mechanics of cellular systems realistically, since, for example, they can involve moving an entire column or row of cells to accommodate a newborn cell, and can therefore contain instantaneous ‘action at a distance’ effects. To overcome such problems, off-lattice models have been developed, which model the behaviour of cells in a far more realistic manner. Of these, there are two general classes of model. In cell-centre models, the location of a cell is given by a single point, its centre, and the total force on any cell is a function of the set of cell centres. In vertex models, each cell is polygonal and defined by the location of a finite set of vertices (see, for example, [4]). Rules are set up to define how any vertex moves, based on (for example) the location

of connecting vertices and the area of neighbouring cells, and further rules are required for cell birth and cell rearrangement.

In this paper we restrict our attention to cell-centre models. There are often two components to such models: (i) a definition of *cell-connectivity*, which, given a set of cell-centre locations, define which cells are in contact; and (ii) a definition of the force between two cells in contact, i.e. the *cell-cell interaction force*.

There are two commonly used methods for determining cell connectivity. In the first, known as the *overlapping spheres* (OS) method, two cells interact if they are within a certain distance of each other. The second method, known as the *Voronoi tessellation* or *triangulation* method, involves computing a triangulation of the domain using the cell centres as nodes. The edges of the resultant mesh define cells in (compressive or adhesive) contact.

For cell-centre models, the cell–cell interaction force is a function of (at least) the location of the cell centres, and nearly always acts in the direction of the vector connecting the two cell centres. The force law can be different depending on whether the cells are in compression or in tension. There are a wide range of force laws that have been used in the

literature, ranging from simple linear laws (with the same stiffness for compression and tension), to much more complex nonlinear models which take into account cell–cell adhesion, cell–substrate adhesion, cell bond breaking, and more.

Let r_k be the position of the k th cell centre, and let \mathbf{F}_{ij} denote the force on cell i due to cell j . As mentioned above, this is usually assumed to act in the direction of the vector connecting the cells, which means that

$$\mathbf{F}_{ij} = F_{ij} \frac{\mathbf{r}_i - \mathbf{r}_j}{\|\mathbf{r}_i - \mathbf{r}_j\|}, \quad (1)$$

where F_{ij} is the signed magnitude of \mathbf{F}_{ij} . The total force on cell i is given by $\mathbf{F}_i = \sum_j \mathbf{F}_{ij}$, where the sum is over all cells j connected to cell i . This force is usually taken to be balanced by a viscous drag as the cells move (that is, the overdamped version of Newton's second law is used in which inertia is negligible) so that

$$\gamma \frac{d\mathbf{r}_i}{dt} = \mathbf{F}_i, \quad (2)$$

where γ is the viscosity coefficient which could, for example, represent adhesion between a cell and the underlying substrate. All our simulations will involve a quasi-steady evolution of the loading, so that the cells reach equilibrium at any given load; in this case (2) can be viewed simply as a numerical method for reaching the next steady state. In our numerical simulations we use a simple forward Euler discretization of (2), so that the position of a cell at time $t + \Delta t$, given its position at time t , is given by

$$\mathbf{r}_i(t + \Delta t) = \mathbf{r}_i(t) + \frac{\Delta t}{\gamma} \mathbf{F}_i. \quad (3)$$

Note that the Euler method is a relatively crude approach to solving (2) and requires small time steps to be trusted. We have verified that the time step chosen, $\Delta t = 10^{-2}$ h, is suitably small. (The simulation run in figure 6(a), which will be discussed later, was rerun with $\Delta t = 5 \times 10^{-3}$ h, and the relative differences in the forces obtained were less than 0.1%).

The cell–cell interaction force is usually a function of the *overlap*, δ_{ij} , between the two cells, and/or their *contact area*, A_c . The overlap between cells i and j whose centres are located at \mathbf{r}_i and \mathbf{r}_j is given by

$$\delta_{ij} = R_i + R_j - \|\mathbf{r}_i - \mathbf{r}_j\|, \quad (4)$$

where R_i and R_j are the natural radii of the cells. Note that the term overlap can be slightly misleading; δ_{ij} is simply the difference between the separation of the cell centres and their ‘natural’ separation, and can be negative if the cells are adhering to each other. In all our simulations we will ignore cell growth and assume a homogeneous tissue, so R_i is constant both in time and over i . We denote this constant by R , so that

$$\delta_{ij} = 2R - \|\mathbf{r}_i - \mathbf{r}_j\|. \quad (5)$$

Different definitions of the contact area are possible, as will be discussed in section 2. We will consider specific examples of F_{ij} in section 2.2.

The aim of this paper is to perform a comprehensive computational study of some of the cell-centre-based mechanical models that are used in the literature. To do

so, we will perform a number of numerical experiments, aimed at replicating typical laboratory experiments used for determining the mechanical properties of a sample of material. As noted earlier, we restrict our attention to the mechanical aspects of the model; we do not include cell birth or model cell growth. This is so that we can study the bulk material properties corresponding to each microscale mechanical model independently of the separate concern of cell proliferation.

Our basic numerical experiments are simple, and represent standard uniaxial compression/tension and shear laboratory experiments. An initial two-dimensional monolayer of 20×20 cells is set up. A two-dimensional tissue is used for computational efficiency (as we have to perform a large number of simulations), and because in 2D it is straightforward to construct an equilibrium starting state. In the uniaxial compression/tension experiments, the top row of cells are displaced a small amount ($0.2R$) in the y -direction. The tissue is then allowed to deform according to (2) and the specified force law, until it reaches equilibrium. In the tension experiments, given normal and zero tangential displacements are specified on the top and bottom surfaces of the tissue, while the sides are stress free. In the compression experiments the tissue is allowed to slide freely against the compressing probe, so that the normal displacement only is given on the top and bottom surfaces, with zero traction there. Once in equilibrium, the force on the compressed/pulled surface is computed as

$$F = \sum_{i \in \mathcal{T}} \mathbf{F}_i \cdot \mathbf{e}_2, \quad (6)$$

where \mathcal{T} is the set of cells in contact with the top surface, and \mathbf{e}_2 is the unit vector in the y -direction. We also compute the force per cell as

$$\hat{F} = \frac{F}{|\mathcal{T}|}, \quad (7)$$

which is a measure of the stress in the material. The tissue is then compressed or stretched further, by again displacing the top row, and the process repeated, providing us with a stress–strain curve. We use the strain $\lambda = l/l_0$, where l_0 and l represent the undeformed and deformed height of the tissue, as the independent variable, and calculate the force required to generate such a deformation. In compression experiments we compress the tissue down to 50% of its initial length. For tension experiments, we stretch the tissue until it tears. We note that similar experiments to this tension experiment have been carried on a computational model of a single cell [5], in which a linear elastic response is observed until breakage or plasticity.

Shear experiments are performed similarly, with the top row of cells repeatedly displaced a small amount ($0.1R$) in the x -direction and fixed in position, and the tissue allowed to deform until it reaches equilibrium.

These experiments will allow us to (i) make some observations on the implementation of these models and (ii) obtain the resultant bulk force laws for tissues under compression, tension and shear (observing how this force law depends on the choice of model), allowing us to gain an insight

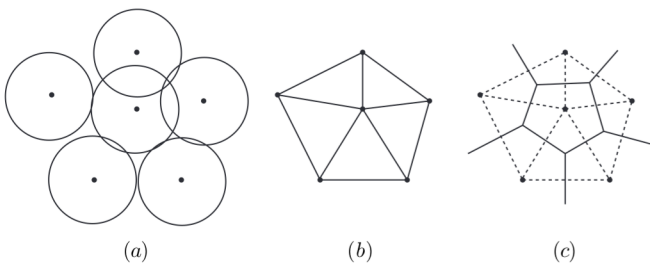


Figure 1. (a) The overlapping spheres method of defining connectivities between cells; (b) the triangulation method of defining connectivities; (c) the Voronoi tessellation corresponding to the triangulation in (b).

into the type of bulk behaviour a multi-cellular tissue possesses when modelled as a collection of interacting cells.

Note that the strains we impose on the tissue are far beyond the strains for which soft tissues deform linear elastically. Although some of the models we study were only proposed for small deformations, and few for the kind of large deformations which we shall force upon them, when modelling growth large strains are necessarily generated, and it is important to understand how the material will respond to such strains. In fact, we shall see that the behaviour of the tissue under large strains is only weakly dependent on the form of the cell-cell interaction law with large δ_{ij} .

We begin in section 2 by describing the methods of defining cell connectivity in more detail, and reviewing various force laws proposed in the literature. Section 3 discusses a few issues that arise when implementing these models. We then investigate the bulk behaviour of the tissue in section 4, first of all studying the deformation in detail and identifying the type of material behaviour which occurs, before performing a comparison of OS versus Voronoi approaches, and a comparison of the different cell-cell interaction laws, in the cases of compression, tension and shear.

2. Models

Most of the cell-centre models which have been proposed in the literature can be classified by a choice of a connectivity law and a force law (though this is not always the case—some models, such as the JKR model (see section 2.2), have force laws that are tightly coupled to a definition of connectivity). Thus we first discuss connectivity options in section 2.1, before discussing force laws in section 2.2.

2.1. Connectivity

As mentioned above, the two most common methods for determining cell connectivity, given a finite set of cell-centre locations, are the overlapping spheres (OS) approach (or extensions on this) and the Voronoi tessellation approach. These are illustrated in figure 1.

In the OS approach, each cell has an intrinsic radius R_c associated with it, and the cells are defined to be connected if the corresponding spheres overlap (figure 1(a)). In other words, two cells interact if and only if they are within a

specified fixed distance of each other. Overlapping cells may not necessarily be in compression—the radius of interaction associated with each cell can be larger than the natural radius of a cell, i.e. $R_c > R$, to allow for adhesive effects to be included. An overlapping spheres approach has been used in models of epithelial monolayers [6–8], tumour spheroids [9], general monolayers and spheroids [10], and general cell-populations [11].

One disadvantage of modelling cells using the OS approach is that real cells are not naturally spherical and a model of spherical cells will not pack as closely as cells in reality. Methods to overcome this issue are using ellipsoids instead of spheres [12], using a polydisperse model (e.g., cells of varying radii) or modelling each cell as a collection of interacting subcellular elements [5], which can lead to much more realistic cellular geometries. For simplicity, in this study we only consider equal radii spheres, and a comparison of the results in this paper with more advanced models is left for future work.

Note that in an OS model, the contact area between two cells can be approximated as the area of the circle of intersection of two spheres. For example, for two spheres of equal natural radius R and with overlap δ_{ij} , the contact area can be approximated as

$$A_c^{\text{sph}} = \pi \delta_{ij} \left(R - \frac{\delta_{ij}}{4} \right). \quad (8)$$

Alternatively, the area of the circle of intersection of two spheres of radius R_c can be used.

In tessellation models, a Delaunay triangulation (see [13]) of the domain is computed using the cell centres, as in figure 1(b). The edges of the triangulation are then used to define connected cells. Such a model of cell connectivity is used in models of intestinal crypts [14] and epithelia [15]. Delaunay triangulations are dual to Voronoi tessellations, as shown in figure 1(c), and the Voronoi region for a given cell centre (the set of points which are closer to that cell centre than any other) can be taken as the definition of the cell itself, i.e. the region in space which is occupied by that cell. This can be convenient for visualization purposes, and also allows the volume of the cell to be defined, as well as providing an alternative definition of the contact area between two cells, which we denote as A_c^{vor} .

A hybrid model is used in [16], where connectivity is defined using an OS model, but—with a note that a Voronoi description has been found in certain cases to approximate cell shapes remarkably well—the contact area between two cells is taken to be the minimum of the spherical and Voronoi contact areas, i.e. $A_c^{\min} = \min \{ A_c^{\text{sph}}, A_c^{\text{vor}} \}$.

Note that both of these definitions of connectivity are purely geometrical. Non-geometrical definitions have also been used. We will discuss the JKR model below in section 2.2, where connectivity is dependent on the history of the tissue. In [17] cells are defined to be connected if their overlap is positive or if they are *bonded*, where cell bonding occurs stochastically every time step, with the probability of two cells bonding being dependent on the distance between the cells and the extracellular calcium ion concentration. Also,

not all models require a definition of cell connectivity: some models (see [18] for a discussion) use a long-range potential with an exponentially decaying tail. In these models only the force law (or equivalently, the potential) is specified, and the decaying tail ensures that the interaction between suitably separated cells is negligible. Such models are therefore similar to OS models, in that there is essentially a fixed region in which cells can interact with a given cell.

2.2. Force laws

A number of cell-cell interaction force laws have been used in the literature. Often the force is taken to be the derivative of a potential (which can be identified as the energy of the interaction). This can allow for example the imposition of a ‘hard-core’ constraint, so that there is a maximum amount of compression possible, by defining the potential to be infinite in some regions [7]. The solution procedure for this type of model is usually stochastic, using the *Metropolis algorithm*, in which a trial displacement in phase-space is chosen at random, and accepted with probability 1 if it decreases the total energy, or accepted with probability $p \equiv p(\Delta W)$ if it increases the total energy by ΔW . Such an approach differs significantly from the deterministic approach outlined in section 1, and a comparison of such models with those which use (2) is beyond the scope of this paper.

We now consider some of the interaction laws which have been used to model compression and adhesion. The simplest possible relationship between force and overlap is the *linear law*,

$$F_{ij} = k_1 \delta_{ij}, \quad (9)$$

where k_1 is a stiffness parameter; this law is used in [6, 7, 14]. Such a law would imply a large attraction between distant cells were it not for the cut-off in the OS model of connectivity. However, no such natural cut-off exists in the Voronoi model of connectivity, and we shall see in section 3 that to get sensible results in this case we must have a force law which is zero for sufficiently well separated cells (i.e., for sufficiently negative overlaps). Thus we also define a *cut-off linear law*

$$F_{ij} = \begin{cases} k_1 \delta_{ij} & \text{for } \delta_{ij} \geq \delta_{\min} \\ 0 & \text{for } \delta_{ij} < \delta_{\min} \end{cases} \quad (10)$$

for some small *cut-off* (or *pull-off*) point $\delta_{\min} < 0$; such a law is used in [17]. The cut-off δ_{\min} is related to the interaction radius R_c in an OS model: $R_c = R - \delta_{\min}$ (i.e., $R_c = R + |\delta_{\min}|$). In [19] the force is taken to be proportional to the contact area rather than the overlap, giving

$$F_{ij} = k_2 A_c. \quad (11)$$

We will also consider the *linear-exponential law*

$$F_{ij} = \begin{cases} k_1 \delta_{ij} & \text{for } \delta_{ij} \leq \delta_c \\ k_1 \delta_c \exp\left(\alpha\left(\frac{\delta_{ij}}{\delta_c} - 1\right)\right) & \text{for } \delta_{ij} \geq \delta_c, \end{cases} \quad (12)$$

where $\alpha > 0$, in which the response is linear up to for some maximum overlap $\delta_c > 0$, and thereafter rises rapidly. In the limit of large α this becomes a hard constraint that the separation can never be less than δ_c , which is sometimes referred to as a hard-core model.

The Hertz theory of contact [20] has also been used in modelling cell interactions [11, 16, 21]. Here, the interaction force is given by

$$F_{ij} = \frac{4\hat{E}}{3\sqrt{\hat{R}}} \delta_{ij}^{\frac{3}{2}}, \quad (13)$$

where

$$\hat{E} = \left(\frac{1 - v_i^2}{E_i} + \frac{1 - v_j^2}{E_j} \right)^{-1}, \quad (14)$$

where E_k and v_k are Young’s modulus and Poisson’s ratio of cell k respectively, and

$$\hat{R} = \left(\frac{1}{R_i} + \frac{1}{R_j} \right)^{-1}. \quad (15)$$

Hertz theory also provides an alternative expression for the contact surface area, $A_c^{\text{Hertz}} = \pi \delta_{ij} \hat{R}$.

A more advanced theory for modelling spherical bodies in contact, the *Johnson–Kendall–Roberts (JKR) theory*, is used in [9] (with a hard-core and the Metropolis algorithm), and investigated experimentally for two adhering cells in [22]. This theory is used to describe elastic isotropic adhesive spheres in contact. Here, the radius of the contact surface, a , is defined and related to the overlap by the expression

$$\delta_{ij} = \frac{a^2}{\hat{R}} - \left(\frac{2\pi\sigma a}{\hat{E}} \right)^{\frac{1}{2}}, \quad (16)$$

(when two cells are in contact), where $\sigma \geq 0$ is the work done by adhesion. The JKR contact area is therefore $A_c^{\text{JKR}} = \pi a^2$. The JKR interaction force is given by

$$F_{ij} = \frac{4\hat{E}}{3\hat{R}} a^3 - (8\pi\sigma\hat{E}a^3)^{\frac{1}{2}}. \quad (17)$$

Note that these equations reduce to the Hertz definitions in the case of $\sigma = 0$. For $\sigma > 0$ we can define $\delta_{\text{typ}} = (\pi\sigma/\hat{E})^{2/3}\hat{R}^{1/3}$, $a_{\text{typ}} = (\pi\sigma/\hat{E})^{1/3}\hat{R}^{2/3}$ and $F_{\text{typ}} = \pi\sigma\hat{R}$, and nondimensionalize by setting $d = \delta_{ij}/\delta_{\text{typ}}$, $A = a/a_{\text{typ}}$ and $f = F_{ij}/F_{\text{typ}}$, to give

$$d = A^2 - \sqrt{2A} \quad (18)$$

$$f = \frac{4}{3}A^3 - \sqrt{8A^3}, \quad (19)$$

which are plotted in figure 2. Note that (unlike any of the previous force laws described) the relationship between F and δ_{ij} is implicit and multivalued, so that care must be taken when using an iterative solution method such as Newton’s method to guarantee convergence to the correct root. The JKR model takes into account hysteresis between the spheres. As two cells come together, the contact area a and therefore the force F_{ij} are zero while $\delta_{ij} < 0$. When two cells come into contact, they spontaneously form a contact surface of finite size ($\delta_{ij} = 0$ but $a > 0$), due to adhesion. If the cells are then pulled apart, the contact area is defined to be non-zero until $\delta_{ij} = -(3^{1/3}/4)\delta_{\text{typ}}$, at which point the cells separate. Note also that, unlike the previous laws, the equilibrium state is not $\delta_{ij} = 0$, but $\delta_{ij} = (3/4)^{\frac{1}{3}}\delta_{\text{typ}} > 0$.

The JKR model provides a natural definition of cell connectivity: any two cells are connected if their contact area $\pi a^2 > 0$.

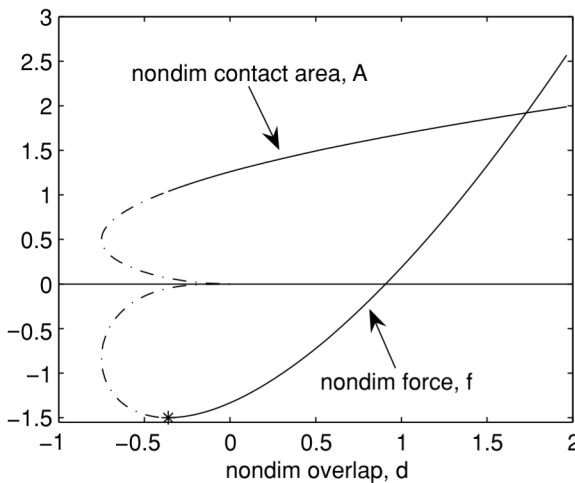


Figure 2. The non-dimensionalized contact area and force, against non-dimensionalized overlap, for the JKR model. The dot-dashed lines indicate continuations of equations (18) and (19) into regions after which the cells have separated.

2.2.1. Adhesion laws. There are a number of possibilities for the force law for cells in adhesive contact. The linear law (10) is defined for all δ_{ij} , and the JKR law is specifically designed for adhering bodies. The Hertz law however does not extend to $\delta_{ij} < 0$. If a force law that is dependent on the contact area rather than the overlap is used, then for the Voronoi model this presents no difficulty, while for the overlapping spheres model the area of overlap must be calculated according to the cells' interaction radius R_c rather than their natural radius R . A linear relationship between force and contact area

$$F_{ij} = k_3 A_c, \quad k_3 > 0, \quad (20)$$

is used in [16], while a linear relationship between the potential and contact area

$$W = k_4 A_c, \quad F_{ij} = \nabla W = k_4 \nabla A_c, \quad (21)$$

where $k_4 > 0$, is used in [9]. The definition of contact area is $A_c = A_c^{\min}$ in [16], and $A_c = A_c^{\text{sph}}$ in [9], although of course

either law could be used with any definition of contact area. Note that in (21), the force is not necessarily in the direction connecting the two cell centres. For this reason we do not include it in any of our numerical experiments.

3. Issues in implementation

The first comment we make on the overlapping spheres approach is the lack of robustness in this type of model. In certain cases, depending on parameter values, the model can display a lack of stability, as illustrated in figure 3, for which an OS model is used with the linear law (10), with the cut-off point δ_{\min} set to be $-R$, and using a tissue with a small number of cells. In this simulation new cells are born as time progresses (using rules defined in [14]). This is the only occasion where we include cell birth in a simulation in this paper. The figure shows the tissue at the beginning of the simulation, when the cells are in equilibrium, and then when a few new cells have been created and the tissue has started to deform, and the resultant breakdown of the model.

This collapse of the tissue occurs essentially because the model allows the possibility of three co-linear, or nearly co-linear, cells all being pairwise connected and exerting forces on each other, when physically the outer cells should not be connected. If the attraction from the next-nearest-neighbour overcomes the repulsion from the nearest-neighbour (recall that there are more next-nearest neighbours than nearest neighbours) then an 'implosion' can occur, as seen in figure 3. From this description it is clear that the form of the force law plays an important role in the stability properties of the model. If the repulsion at small separation is sufficiently strong then such implosions do not occur; this is an argument against the naive use of a linear force law.

Note that this issue has not arisen in previous work using a linear force law and overlapping spheres [6, 7]; this is can be partly attributed to the fact these models are simulated in one dimension only. Although we have illustrated the instability using cell birth, it can be expected that linear-force-law OS models will also fail under suitably high compression, since

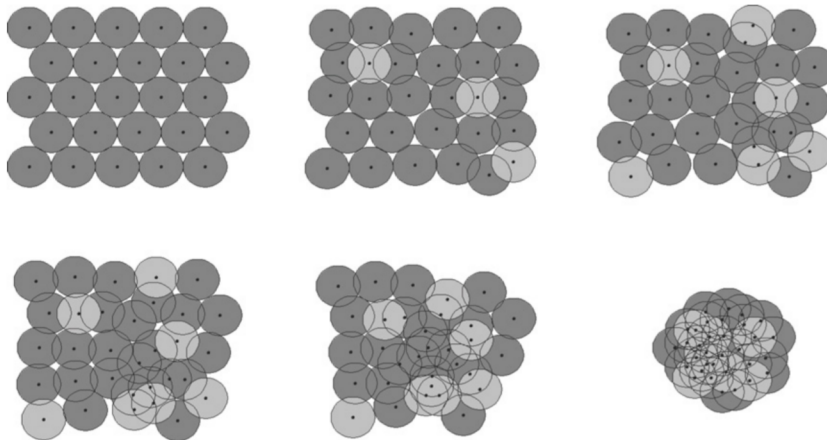


Figure 3. The onset of instability with an overlapping spheres model. Time increases left to right and then top to bottom. (Note that the shaded region for each cell represents the cell's natural radius, rather than the maximum radius of interaction, and progeny are shown in lighter grey). The cells are initially in equilibrium, but the birth of a few cells eventually leads to breakdown of the model.

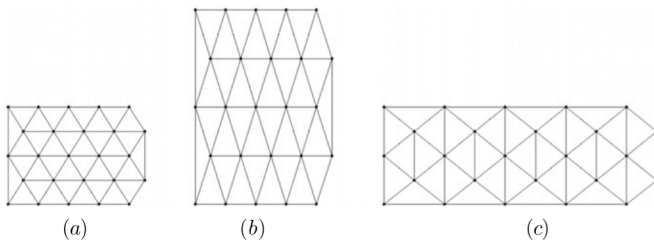


Figure 4. (a) An initial ‘honeycomb’ mesh of equilateral triangles, representing a tissue with all cells that are connected the same distance away from each other. (b) If this mesh is stretched in the y -direction, and retriangulated, the same cells will be connected, no matter how much the mesh is stretched. (c) However, if the mesh is stretched enough in the x -direction and retriangulated, new connections are created. The opposite applies for compression.

in that case also cells will begin to form connections with next-nearest neighbours; cell birth is simply an obvious way of creating large local distortions of the tissue.

The possibility of connections with next-nearest neighbours, and the resulting stability problems, is one of the reasons the Voronoi approach to cell connectivity has been proposed, as performing a triangulation of the domain is an elegant way of avoiding the issue of three nearly collinear cells being pairwise connected. Indeed, the same simulation as that in figure 3, with the same parameters but using a Voronoi definition of connectivity, does not display instabilities. However, the Voronoi approach has its own implementation problems. One issue with Voronoi models is the boundary of the tissue—since a Delaunay triangulation of a set of points results in a triangulation of the *convex hull* of the points, a basic Delaunay triangulation of a set of cell centres will invariably lead to distant boundary cells being erroneously connected. Such issues are not discussed in [14] or [15]⁴. One way to avoid this is to introduce a cut-off distance, i.e. a maximum distance between cell centres beyond which cells are defined to be not connected.

A more subtle issue that is worth noting is displayed in figure 4. Figure 4(a) displays an initial set of cell-centres forming a ‘honeycomb’ mesh where every point is of equal distance to all connected points (and therefore with all cells in equilibrium), which is a sensible starting state for the numerical experiments performed in this paper. Only a small tissue sample of 5×5 cells is used for clarity in these images. Figure 4(b) shows the mesh scaled in the y -direction and retriangulated—the cell connectivity as defined by the new Delaunay triangulation is identical to the starting state. This is true for any amount of stretching of the mesh in this direction. However, if the mesh is stretched enough in the x -direction instead, there is a point when new connections are formed, as shown in figure 4(c). The converse applies for compression—new connections will form if the mesh is compressed enough in the y -direction, but not if it is compressed in the x -direction. In principle this lack of isotropy could lead to anisotropic material properties. On the other hand, although a highly stretched hexagonal mesh is a possible solution configuration, we would expect in practice that the cells would intercalate.

⁴ A cylindrical geometry with fixed cells at the bottom surface is used in [14], but the issue still applies to the top surface.

Table 1. Parameter values used for the numerical experiments.

Parameter	Value	Reference
Viscosity, γ	$0.4 \text{ N s}^{-1} \text{ m}^{-1}$	[11]
Cell radius, R	$5 \times 10^{-6} \text{ m}$	[9]
Linear law parameter, k_1	$2.2 \times 10^{-3} \text{ N m}^{-1}$	Chosen
Linear in contact area parameter, k_2	149 N m^{-2}	Chosen
Linear to exponential max. overlap, δ_c	$2 \times 10^{-6} \text{ m}$	Chosen
Linear-exponential law parameter, α	1	Chosen
Minimum interaction overlap, δ_{\min}	-4×10^{-6}	Chosen
Youngs modulus, E_i	1 KPa, for all cells	[11]
Poisson’s ratio, ν_i	$\frac{1}{3}$, for all cells	[11]
JKR work of adhesion, σ	$1.07 \times 10^{-4} \text{ kg s}^{-1}$	[9]

We will see in the next section that this is indeed what happens, with rearrangements near the boundary eventually penetrating throughout the tissue.

4. Bulk material behaviour

The connectivity models allow cell connectivities to vary with time and therefore allow the structure of the tissue to change under applied loads, so that the bulk material behaviour of the tissue has the potential to be very different to the cell–cell interaction law. To investigate this, we perform a compression experiment, as described in section 1. For this initial experiment, we choose the Voronoi approach for the connectivity model, and use the linear force law (10). The value of k_1 used is that given in table 1 (discussed later) and $\delta_{\min} = -0.4R$.

Figure 5 shows the structure of the tissue at a sample of times during the experiment. Since a Voronoi model is used, the two-dimensional area representing each cell can be plotted, by taking the Voronoi tessellation corresponding to the underlying mesh. Both the mesh and tessellation can be used to visualize the connectivities in the tissue. In figure 5(a) ($\lambda = 0.99$) and 5(b) ($\lambda = 0.83$), the cell-connectivities are identical, i.e. the tissue has maintained its initial structure. By contrast, a large deformation has occurred by $\lambda = 0.66$, as shown in figure 5(c). Here, a new regular lattice of 23×18 cells has formed, which means that a global rearrangement has occurred, not just local rearrangement. Further local rearrangements are visible in figure 5(d) ($\lambda = 0.5$).

The force-displacement profile for this experiment is shown in figure 6(a). We see that, as the stretch factor decreases, the tissue initially behaves as a near-linear elastic material. This is true for $\lambda > 0.74$, and corresponds to the range of compressions for which the internal structure of the tissue does not change from its initial configuration. For $\lambda < 0.74$, new connections form between the cells, and the tissue deforms to relieve the stress. From this point, the tissue behaves as a plastic material. The force at which yielding occurs is approximately 10^{-7} N . In the plastic regime, the force is no longer monotonic in the compression, and goes through a period of alternatively increasing and decreasing

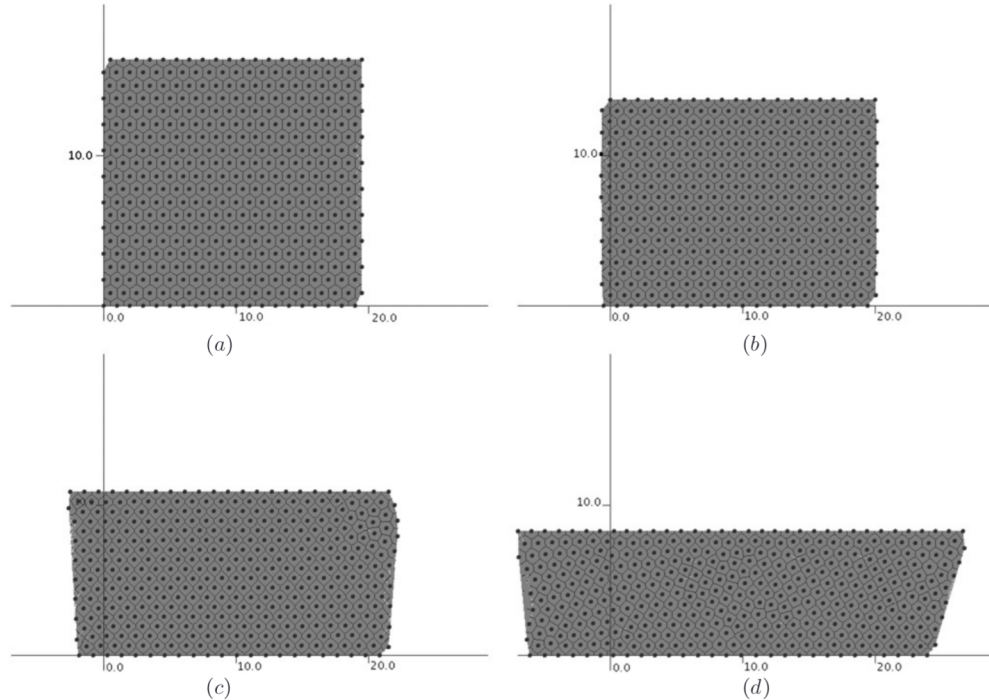


Figure 5. A Voronoi model of 20×20 cells in various degrees of compression. Here we show the Voronoi area associated with each cell. The levels of compression are (a) 0.99; (b) 0.83; (c) 0.66; (d) 0.5.

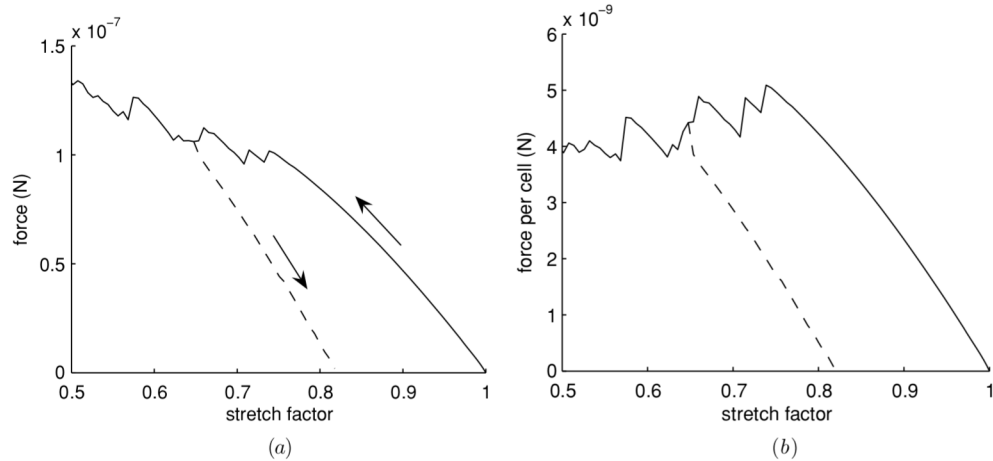


Figure 6. (a) Force against stretch factor as a monolayer sample of tissue is compressed, using a Voronoi model with a linear force law (10). The solid line represents an experiment where the tissue is incrementally compressed to $\lambda = 0.5$. The dashed line represents an experiment where the tissue is compressed to $\lambda = 0.65$ and the compression then incrementally relaxed until there is near zero force. (b) The equivalent force per cell against stretch factor.

with increased compression. To determine the type of plastic behaviour, we also plot \hat{F} , the force per cell (defined in (7))—which is proportional to stress—against the stretch factor, in figure 6(b). The force per cell oscillates for $\lambda < 0.74$, but overall the tissue exhibits slight softening (decrease in stress with increased strain). However, the stress only decreases by a factor of less than 20% from $\lambda = 0.74$ to $\lambda = 0.5$ —in other words, the material behaves similarly to a perfect plastic whilst in the plastic phase. In figure 7(a)–(d), the connectivity is again plotted at a selection of times, but now using the mesh rather than the Voronoi tessellation. In this figure, cells which are connected by an edge in the mesh but are far enough apart for there to be zero force (according to (10)) are not

shown as connected. It can be seen that the tissue still has its initial, regular, structure when $\lambda = 0.8$, whereas some small connectivity changes occur when $\lambda = 0.7$ (plastic phase), and much larger changes for $\lambda = 0.6$ and 0.5.

To further investigate the plastic nature of the material, we perform a second experiment when the tissue is compressed as before up to $\lambda = 0.65$, and then incrementally unloaded. This is also plotted in figures 6(a) and (b). Together, the curves form a hysteresis curve for a monolayer tissue under slow compression. During unloading, the tissue again behaves as a linear-elastic solid, with the same Young's modulus as during the loading elastic phase (as the gradients for the initial loading and unloading stages in figure 6(b) are the same).

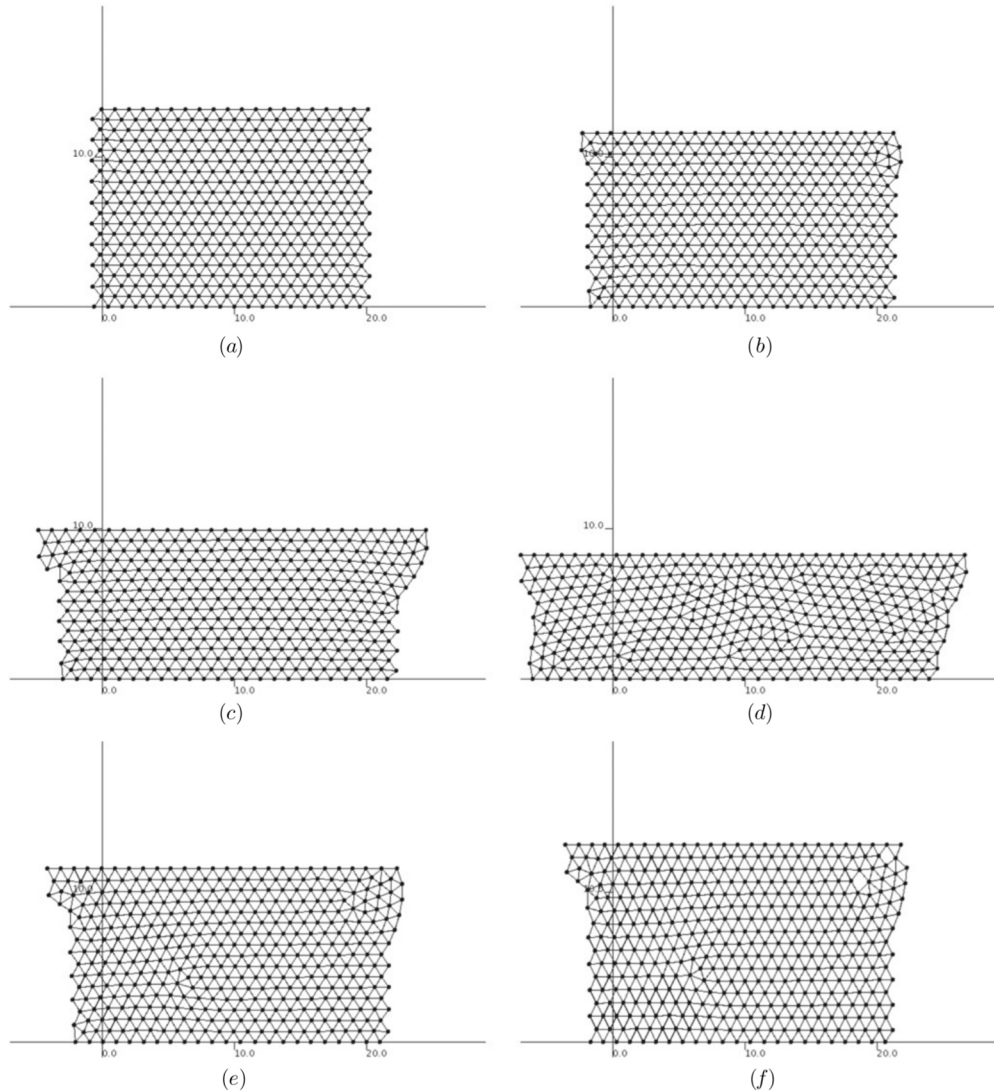


Figure 7. Cell connectivities during a compression experiment (a)–(d), and a compression experiment with unloading (e) and (f), using a Voronoi model and linear force law (10). The levels of compression are $\lambda =$ (a) 0.8; (b) 0.7; (c) 0.6; (d) 0.5; (e) 0.7 during unloading; (f) 0.8 during unloading.

Figures 7(e) and (f) show the structure of the tissue during unloading. Comparing these to figure 7(c), we see that a very small amount of local rearrangement does occur during the unloading stage, but the internal structure does not significantly change.

4.1. Compression

We now compare the Voronoi approach with the overlapping spheres approach for a tissue under compression, by repeating the first experiment with the latter connectivity model. The results are displayed in figure 8. With the OS model, the material also behaves as an elastic–plastic. In the elastic regime, the behaviour is identical to the Voronoi model, except for yielding occurring fractionally earlier with the OS model. In contrast to the elastic regime, the profile in the plastic regime differs significantly to the Voronoi case. The force in the OS case is less than the corresponding Voronoi force throughout the plastic phase and the OS model exhibits a steep drop in the force near $\lambda = 0.6$.

Next, we focus our attention on the choice of law used for the compressive part of the cell–cell interaction force. We will compare the linear law (10), the linear in contact area law (11) (using $A_c = A_c^{\text{sph}}$ (8)), linear-exponential law (12), Hertzian law (13) and JKR law (16) and (17). For these experiments, we choose a Voronoi model, since Voronoi models appear to be slightly superior to overlapping spheres models, except for with the JKR model, where a spherical definition is more natural. For consistency, for the adhesive part of the law, we always use a simple linear model (10), with $\delta_{\min} = -0.4R$, except for the JKR model, which takes into account adhesion. The parameters used are given in table 1⁵.

⁵ Note that the references which use laws (10) or (11) do not provide experimentally derived parameter values for k_1 or k_2 . We have computed k_1 using the value chosen in [14] (using our choice of γ), but this value was found to result in unstable simulations (since the forward Euler method is used, the computations are expected to become unstable if the time step—or equivalently, the stiffness—is too large). A smaller value of k_1 of the same order of magnitude was chosen. In [19], where law (11) is used, the constant of proportionality is not stated, so we have chosen k_2 such that the forces computed using (10) and (11) are equal when $\delta_j = 0.05R$.

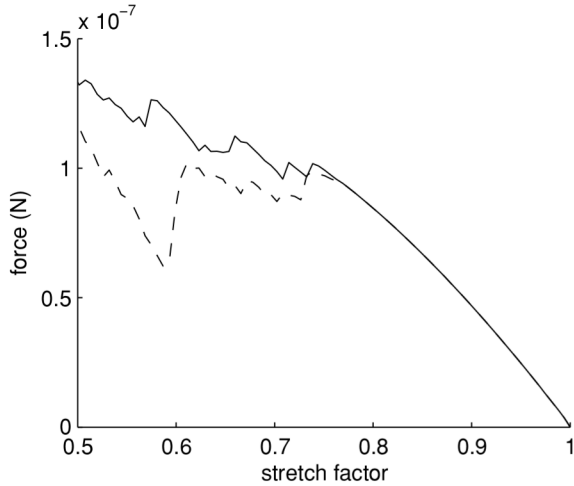


Figure 8. Force against the stretch factor using a linear force law (10) and a Voronoi definition of connectivity (solid line), compared to an overlapping spheres definition of connectivity (dashed line).

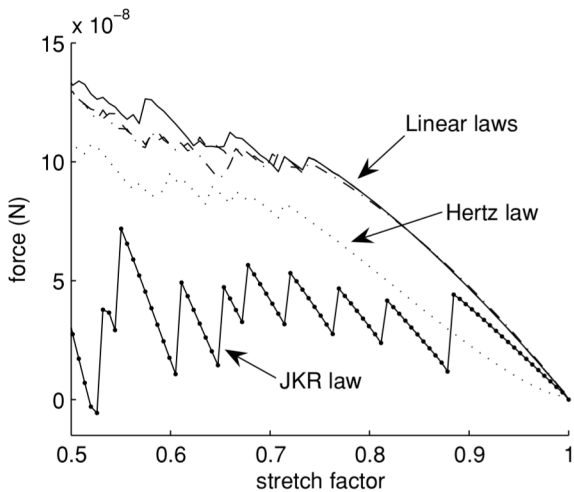


Figure 9. Force against stretch factor as a monolayer sample of tissue is compressed, for various force laws: linear law (10) (solid); linear in contact area law (11) (dot-dashed); linear-exponential law (10) (dashed); Hertzian law (13) (dotted); JKR law (17) (solid line with dots)

The results are displayed in figure 9, which shows some interesting results. The three linear laws (10), (11) and (12) all provide very similar force laws, with the force almost identical while the tissue behaves elastically. For $\lambda < 0.74$, cells form new connections, allowing the tissue to deform and reduce the stress. Even in this region, the difference between the linear laws is not especially large, and for each the force oscillates but overall gradually increases. In figure 10 we plot the force per cell, \hat{F} , and compare it with the value of the corresponding cell-cell interaction force. This figure illustrates how the various cell-cell interaction forces differ greatly for large compressions, but this variation does not affect the resultant tissue force law. In particular, it can be seen that the ‘hard-core’, which was modelled by the exponential part of the linear-exponential law, does not have a significant effect on the tissue force law.

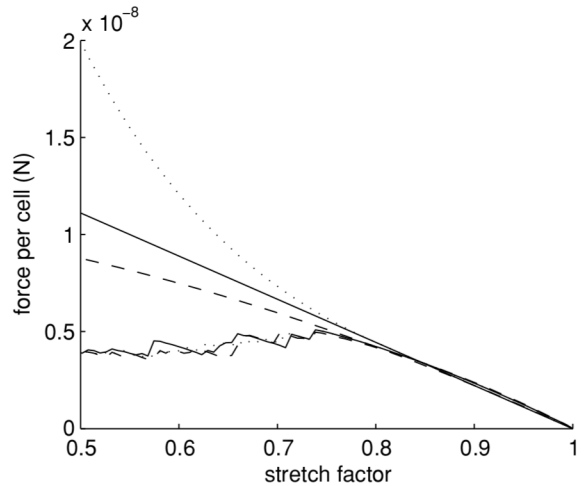


Figure 10. Comparison of the bulk tissue force law (the 3 lower, jagged, curves) and the corresponding cell-cell interaction force (the three higher, smooth, curves). Solid lines: linear law (10); dashed lines: linear-in-contact-area-law (11); dotted lines: linear-exponential law (12).

The forces computed using the Hertzian model, as shown in figure 9, are smaller in magnitude than the linear results, but it is the shape of the curve which is of more interest. Whilst the linear laws were concave for small enough compression, the Hertzian force law is initially convex, with the stiffness increasing with increased compression, as it does in the Hertzian interaction law (13). Again, the tissue behaves as a elastic-plastic, and it is interesting that the yield point is similar to the yield point for the linear models, about $\lambda = 0.72$. A comparison of the force per cell against the Hertzian interaction force is given in figure 11(a), which shows that the Hertzian model also exhibits slight softening in the plastic phase, although in this case the tissue is closer to a perfect plastic.

Surprisingly, the results using the JKR model are very different and appear unrealistic. Here, the cells regularly deform to an extent that the stress sometimes can be almost completely relieved, and at much lower strains—the yield stretch for the JKR model is near $\lambda = 0.9$, in contrast to a value near 0.75 for the other models. The large deformations the tissue undergoes is illustrated in figure 12 which shows the equilibrated tissue at a variety of compressions. At $\lambda = 0.9$ the tissue has not deformed except outwards, as seen by the fact that there are still 20 cells on the top surface. However, at $\lambda = 0.8$, the tissue has already been able to deform to such an extent that a new regular lattice with 24 cells on the top surface has formed, which reduces the compression of each of the cells. By $\lambda = 0.6$ a lattice with 35 cells on the top layer has formed. A comparison of the force per cell against the JKR interaction force is given in figure 11(b).

Investigating this behaviour of a JKR-tissue further, we have repeated this experiment with a modified value of σ in (17), using σ twice the value stated in table 1, representing increased adhesion. This is plotted in figure 13(a), which shows that the JKR model can exhibit very different behaviour depending on the choice of σ (given this choice of \hat{E}). When

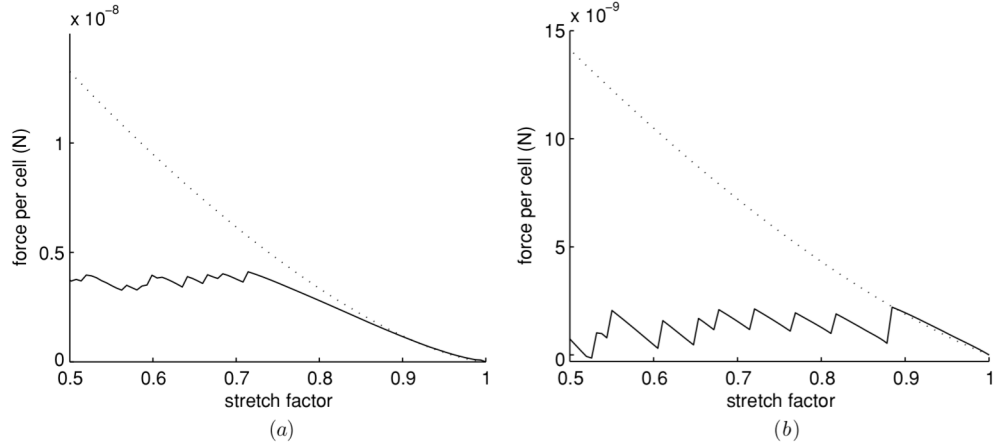


Figure 11. Comparison of the bulk tissue force law (solid lines) and the corresponding cell–cell interaction force (dotted lines) for (a) a Hertzian model; (b) a JKR model.

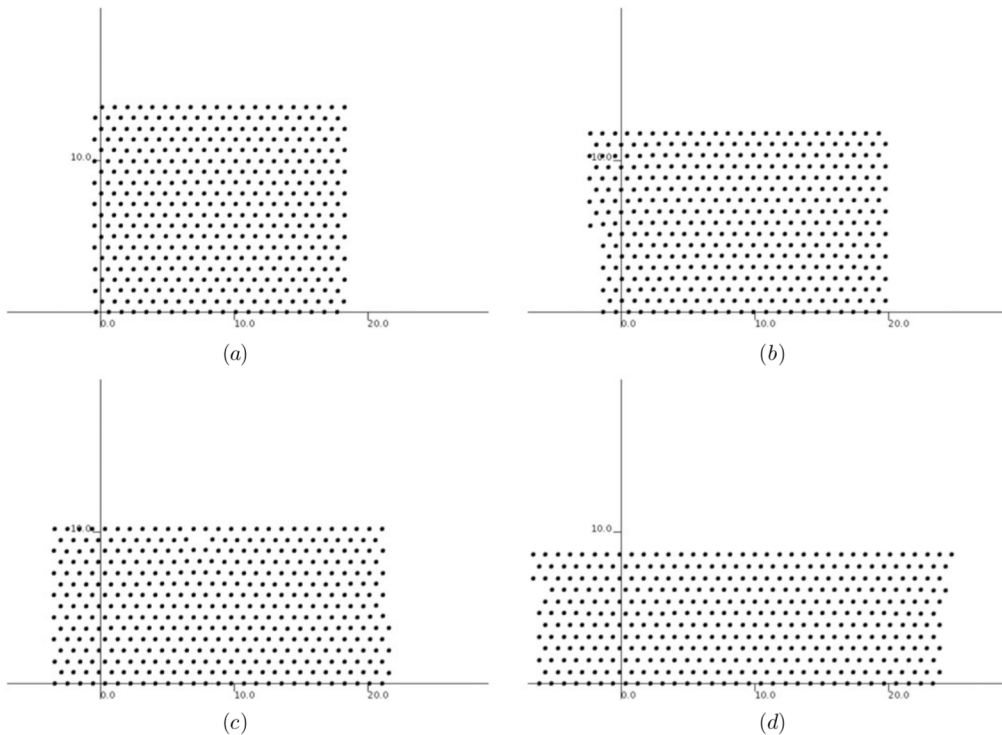


Figure 12. Equilibrated tissue at various levels of compression for the JKR model. $\lambda = (a) 0.9; (b) 0.8; (c) 0.7; (d) 0.6$.

σ is doubled, the tissue no longer deforms to (near-)zero stress states.

Motivated by this result, we perform a final compression experiment where we use a linear law and vary δ_{\min} , in order to investigate the effect of the maximum adhesive interaction distance on the yield strain. The results of this experiment are given in figure 13(b). It can be seen that this parameter plays a crucial role in determining not just the onset of the plastic regime, but also the entire material behaviour. For $\delta_{\min} = -0.1R$ and $\delta_{\min} = -0.2R$ the tissue goes through stages of large increases and decreases in the force, and for $\delta_{\min} = -0.1R$ the tissue can deform into near zero-stress states. However, for $\delta_{\min} = -0.4R$ and $\delta_{\min} = -0.8R$, the tissue behaves as an elastic–plastic with slight softening.

These results are counter-intuitive (adhesion might be thought to be important in determining the behaviour under tension but less so under compression), and show that care must be taken with the choice of this parameter.

4.2. Tension

We now look at the behaviour of the tissue under tension. We use a similar experimental set-up to section 4.1, the only differences for this experiment being that we displace the top row of cells upwards (again, in increments of $0.2R$), and then fix them in place (i.e., do not allow slip), and only stretch the tissue until tearing occurs.

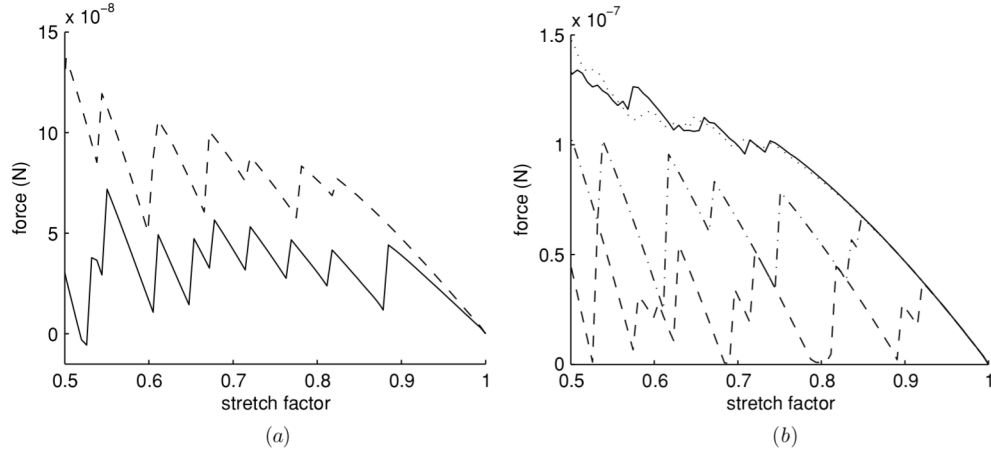


Figure 13. (a) Force against stretch factor with the JKR model, with $\sigma = 1.07 \times 10^{-4} \text{ kg s}^{-1}$ (as in table 1) (solid line); and $\sigma = 2.14 \times 10^{-4} \text{ kg s}^{-1}$ (dashed line). (b) Force against stretch with a linear model and $\delta_{\min} = -0.1R$ (dashed line); $\delta_{\min} = -0.2R$ (dot-dashed line); $\delta_{\min} = -0.4R$ (solid line); $\delta_{\min} = -0.8R$ (dotted line).

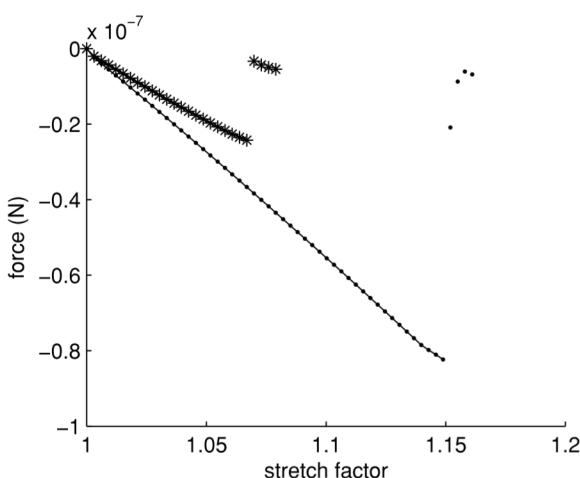


Figure 14. Force against stretch factor as a monolayer sample of tissue is stretched, for linear law (10) (curve with dots) and the JKR law (17) (curve with stars).

Since the three linear laws only differ in the compressive regime, we do not consider (11) or (12). We compare the linear model, again with $\delta_{\min} = -0.4R$, and the JKR model, the results of which are plotted in figure 14.

The linear model has a force-displacement profile which is close to being linear, until tearing occurs for $\lambda \approx 1.15$, where the force decreases suddenly. Note that this value of λ is less than the breaking point of the cell-cell interaction law (with $\delta_{\min} = -0.4R$ two cells would separate at $\lambda = 1.2$). The gradient of the near-linear part of the curve decreases just before tearing occurs, which is because of some initial bond-breaking. Note that when the tissue tears, the force does not immediately decrease to zero. This is due to the tissue not tearing completely into two unconnected regions, and instead just tearing internally, as shown in figure 15. If the tissue was stretched further, it will eventually tear completely, allowing the upper region to deform until the force is zero. Figure 16(a) compares the force per cell on the top of the tissue with the original linear cell-cell interaction law, clearly illustrating that

the tissue tears before the cut-off point for two cells. Also, the stiffness of the bulk tissue is shown to be greater than that of a single cell.

Returning to figure 14, the JKR model also has a force-displacement profile which is close to being linear, although here the stiffness decreases slightly with increased tension. Tearing occurs at $\lambda \approx 1.06$. Figure 16(b) compares the bulk tissue force law for the JKR model with the corresponding force acting between two JKR cells, assuming the two cells are already in contact. It can be seen that, again, the tissue tears at a value of λ which is less than the value of λ which corresponds to the cut-off point in the cell-cell interaction law.

Overall, the tissue in all cases acts as a brittle linear elastic solid, with tearing occurring before any re-triangulation or rearrangement takes place, i.e. before any plastic effects can occur. Since no rearrangement occurs, it might be expected that the use of an OS model does not affect the results. This has been numerically verified to be the case—a simulation using overlapping spheres and the linear force law provides an identical force-displacement profile.

4.3. Shear

Finally, we investigate the material behaviour under shear. Here, in each increment, we displace each cell in the top row by $0.1R$ in the horizontal direction, fix the top and bottom cells in place, and allow the tissue to deform until equilibrium, measuring the force in the horizontal direction. We use a Voronoi definition of connectivity, and the linear force law (10), with $\delta_{\min} = -0.4R$. Let \hat{d} represent the prescribed displacement of the top row of cells, scaled by $2R$ (i.e. a cell's diameter). Figure 17 plots the force against \hat{d} and figure 18 gives the connectivities in the tissue at a selection of \hat{d} . In this case we only present results for this single choice of model. However, we have numerically verified that the use of an overlapping spheres model provides identical results to the Voronoi model, as was the case with compression in the elastic phase and with tension.

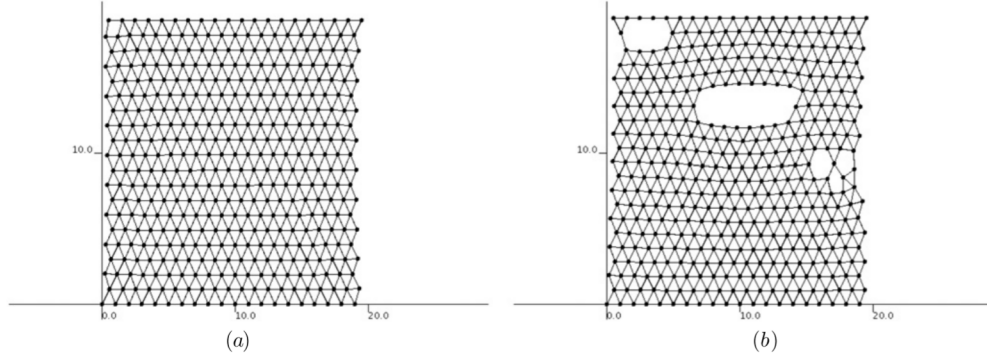


Figure 15. Connectivity of cells in a stretched Voronoi tissue (using a linear force law), just before and after tearing occurs: (a) $\lambda = 1.14$; (b) $\lambda = 1.15$.

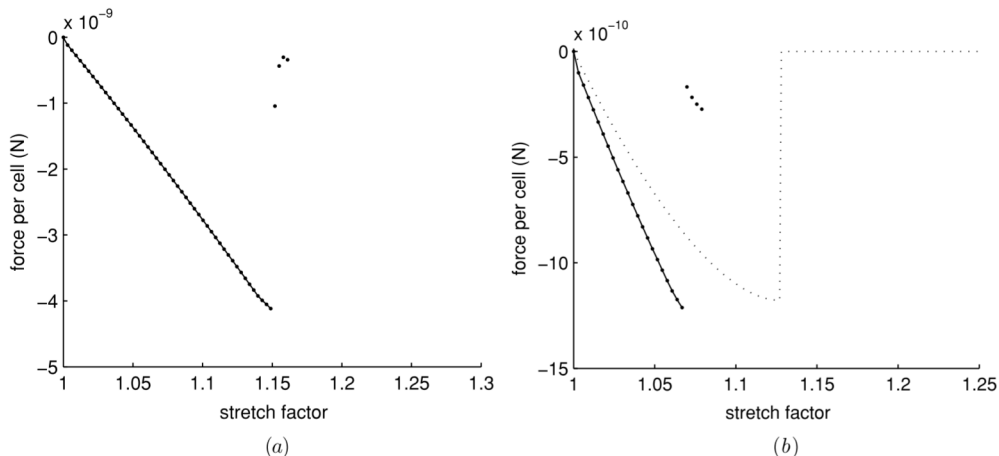


Figure 16. Comparison of the bulk tissue force law (solid lines) and the corresponding cell-cell interaction force (dotted lines) for (a) a linear model under tension; (b) a JKR model under tension.

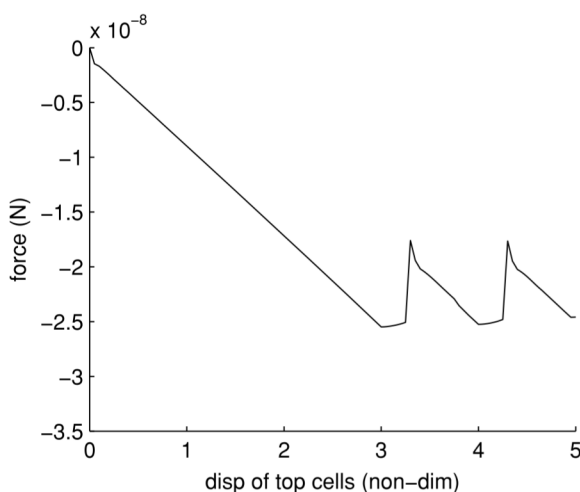


Figure 17. Force against displacement as a monolayer tissue is sheared. The displacement is the prescribed displacement of the top row of cells, scaled by a cell's diameter.

Initially, the tissue deforms without internal rearrangement as the free cells are pulled across by the top row of cells, and the relationship between the \hat{d} and force (or stress) for $\hat{d} < 3$ is completely linear. However, the tissue is too weak to accommodate a large amount of shear: just after $\hat{d} = 3$,

bonds start breaking (as illustrated in figure 18(c)). As the top row of cells is moved further across, more bonds between this row and the second row are broken, and eventually the second row slips across by one cell (figure 18(d)). This results in a new regular lattice with a displaced top row. Note that no rearrangement or plastic deformation occurs anywhere else in the tissue. The process is then repeated as the top row of cells is displaced further (figures 18(e) and (f)). This leads to a pseudo-periodic form of the force in figure 17 for $\hat{d} > 3$, with period 1 (in \hat{d}), or $2R$ in physical units, and means the tissue is kept at around a maximum shear as the prescribed shear displacement is increased. If the process is continued further the top row of cells will eventually become disconnected from the remainder of the tissue. Note again that these results will be highly dependent on δ_{\min} .

5. Conclusions and outlook

This paper has been concerned with the mechanical behaviour of discrete tissue models. Such models have two components, an overlapping spheres or Voronoi definition of connectivity, and a cell-cell interaction force law. We have performed a series of numerical experiments, in which a virtual tissue is slowly and incrementally compressed, stretched and sheared. The tissue is allowed to deform until it reaches equilibrium in

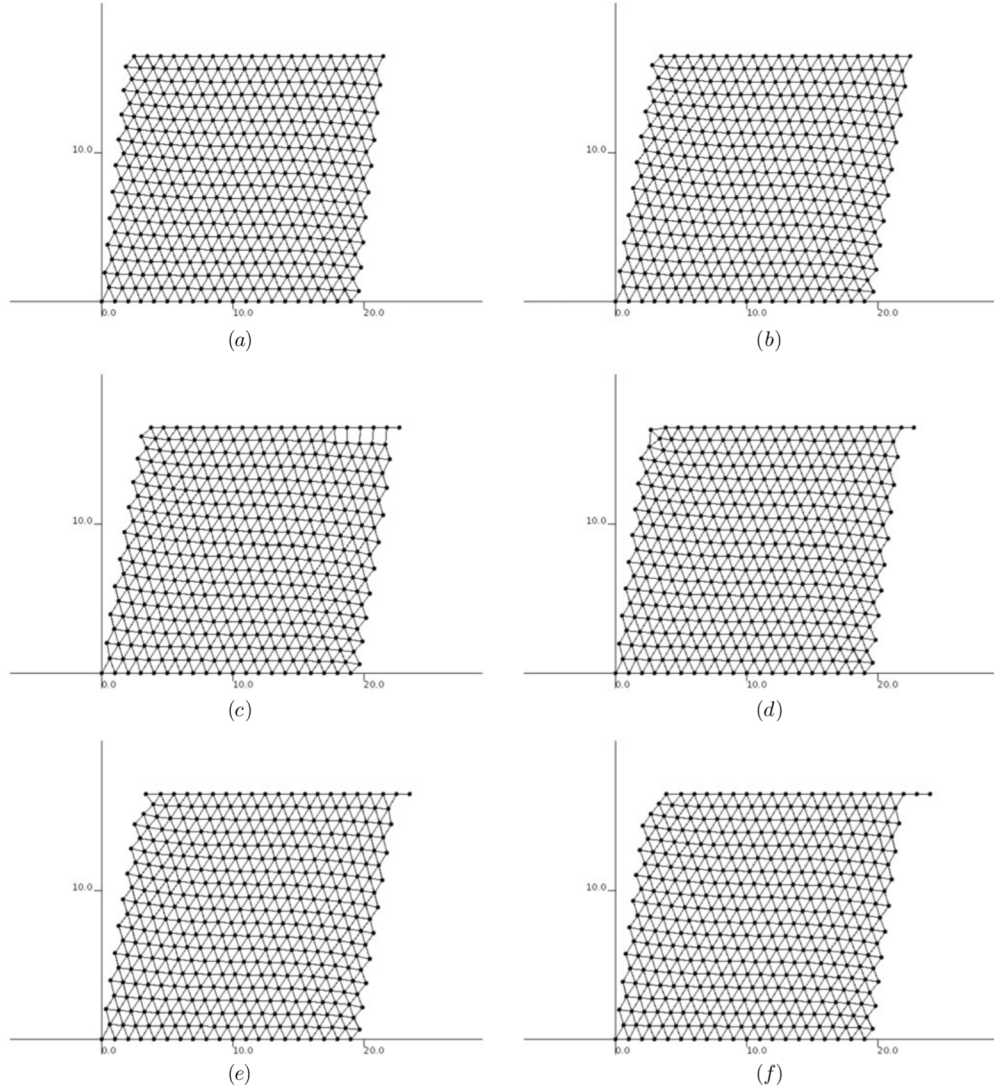


Figure 18. The structure of the sheared tissue for a selection of displacements. The prescribed displacement of the top row of cells, scaled by a cell's diameter, is (a) 2; (b) 3; (c) 3.25; (d) 3.3; (e) 4; (f) 4.5.

each increment, and the force in the loaded direction measured. Since our aim is an in-depth analysis of the passive mechanical response of such models, we have intentionally excluded active cellular features such as cell growth or cell division. We have also not included interaction laws which are defined using a potential that is infinite for suitably high compressions, nor have we studied the corresponding stochastic Metropolis algorithm for solving systems with such laws, or included any other stochasticity in the models. In future work in this area, we aim to investigate the effect on the results in this paper of heterogeneous material parameters, of a stochastic solution procedure, and of the use of vertex models instead of a cell-centre approach.

We have shown that, under slow compression, the tissue initially deforms elastically up to a certain strain, then flows plastically. In the plastic phase, the tissue exhibits slight plastic softening. If the tissue is compressed until it behaves plastically and then unloaded, it immediately returns to an elastic solid of the same stiffness. It was shown that the adhesion parameter δ_{\min} plays an important part in governing

the behaviour under compression. The tissue behaves as a brittle linear elastic solid under tension, tearing before the point that would be predicted using the cut-off point in the cell-cell interaction law, and before any plastic effects can occur. It can withstand a small amount of shear, before local rearrangement occurs. We have shown that the use of an overlapping spheres model instead of a Voronoi model has little effect on the results for compression during the elastic phase or on the yield stress; it has a more noticeable effect during plastic flow, with cell rearrangements leading to larger variation in the stress for overlapping spheres. The overlapping spheres model gives identical results to the Voronoi model when the tissue is under tension or sheared. Thus it seems that an OS approach may be preferable (since it is more efficient), providing the force law is chosen to avoid instability.

Apart from possible instabilities, the choice of cell-cell interaction law has been seen to typically not play an important role in governing the bulk behaviour, and in particular, the form of the cell-cell interaction law for large compressions does not significantly affect the material properties of the tissue under

large compressions (in contrast to adhesion parameters). The JKR model was also shown to be highly dependent on adhesion parameters, with the initial choice of parameters (taken from values used in the literature) leading a tissue which flowed plastically at much smaller strains and was able to regularly deform to a near stress-free state.

In this paper, we have only considered 2D tissues, and it is yet to be verified that the same results are observed in 3D. We would expect the same kind of qualitative behaviour (and in particular, elastic–plastic deformation), but we might expect that the results differ quantitatively—for example, the extra freedom in three dimensions might allow the tissue to deform plastically earlier than in 2D.

This work has aimed to begin to compare the mechanical properties of the very large number of discrete tissue models that have been proposed in the literature. The types of numerical experiment that we have performed can be used to decide if a model behaves in a mechanically realistic manner, and, if it does, to compare the model to experimental results and either verify the model or fit parameters. This experimental comparison is the most important next step—we need to verify whether the elastic–plastic (with slight softening) behaviour predicted by these cell-centre models is observed when small numbers of real cells are slowly compressed. However, we have only considered one of the three main types of discrete model—we have not considered lattice-based or vertex models—and also only considered simplified versions of the cell-centre models that are available, and therefore there is also a great deal of work left in performing an exhaustive comparison.

Acknowledgments

PP is pleased to acknowledge the support of the EPSRC through grant EP/D048400/1, *New frontiers in the mathematics of solids*.

Glossary

Cell-centre model. An off-lattice discrete model in which cells are modelled as point masses at their centres.

Perfect plastic. A plastic material which maintains constant total stress when it is flowing plastically.

Plasticity. Plastic materials deform irreversibly (or ‘flow’) when under critically large stresses, as opposed to elastic materials, which change temporarily during loading but revert back to their original form when unloaded.

Plastic softening. Plastic softening refers to plastic flow where the total stress decreases with increased strain. The opposite is known as plastic hardening.

Voronoi tessellation. A polygonal tessellation of a region containing a set of nodes in which the polygon corresponding to a given node contains all points closer to that node than any other. It is dual to a Delaunay triangulation. Hence, given a set of nodes representing cell centres we can use a Delaunay

triangulation to determine cell connectivity and the polygons in the Voronoi tessellation to represent the actual cells.

References

- [1] Moreira J and Deutsch A 2002 Cellular automaton models of tumor development: a critical review *Adv. Complex Syst.* **5** 247–67
- [2] Dütchting W and Vogelsaenger T 1985 Recent progress in modelling and simulation of three-dimensional tumor growth and treatment *BioSystems* **18** 79–91
- [3] Qi A, Zheng X, Du C-Y and An B 1993 A cellular automaton model of cancerous growth *J. Theor. Biol.* **161** 1–12
- [4] Farhadifar R, Röper J, Aigouy B, Eaton S and Jülicher F 2007 The influence of cell mechanics, cell-cell interactions, and proliferation on epithelial packing *Curr. Biol.* **17** 2095–104
- [5] Sandersius S and Newman T 2008 Modeling cell rheology with the subcellular element model *Phys. Biol.* **5** 015002
- [6] Drasdo D and Loeffler M 2001 Individual-based models to growth and folding in one-layered tissues: intestinal crypts and early development *Nonlinear Anal.* **47** 245–56
- [7] Drasdo D 2000 Buckling instabilities in one-layered growing tissues *Phys. Rev. Lett.* **84** 4244–7
- [8] Drasdo D and Forgacs G 2001 Modeling the interplay of generic and genetic mechanisms in cleavage, blastulation and gastrulation *Dev. Dyn.* **219** 182–91
- [9] Drasdo D and Holme S 2005 A single-cell-based model of tumor growth *in vitro*: monolayers and spheroids *Phys. Biol.* **2** 133–47
- [10] Drasdo D, Hoehme S and Block M 2007 On the role of physics in the growth and pattern formation of multi-cellular systems: what can we learn from individual-cell based models *J. Stat. Phys.* **128** 287–345
- [11] Galle J 2005 Modeling the effect of deregulated proliferation and apoptosis on the growth dynamics of epithelial cell populations *in vitro* *Biophys. J.* **88** 62–75
- [12] Pallson E 2001 A three-dimensional model of cell movement in multicellular systems *Future Generation Comput. Syst.* **17** 835–52
- [13] Delaunay B 1934 Sur la sphère vide *Izvestia Akademii Nauk SSSR, Otdelenie Matematicheskikh i Estestvennykh Nauk* **7** 793–800
- [14] Meineke F, Potten C and Loeffler M 2001 Cell migration and organization in the intestinal crypt using a lattice-free model *Cell Prolif.* **34** 253–66
- [15] Morel D, Mercelpoil R and Brugal G 2001 A proliferation control network model: the simulation of two-dimensional epithelial homeostasis *Acta Biotheoretica* **49** 219–34
- [16] Schaller G and Meyer-Hermann M 2005 Multicellular tumor spheroid in an off-lattice Voronoi-delaunay cell model *Phys. Rev. E* **71** 051910
- [17] Walker D, Southgate J, Hill G, Holcombe M, Hose D, Wood S, MacNeil S and Smallwood R 2004 The epitheliome: agent-based modelling of the social behaviour of cells *BioSystems* **76** 89–100
- [18] Newman T 2008 Grid-free models of multicellular systems, with an application to large-scale vortices accompanying primitive streak formation *Curr. Top. Dev. Biol.* **81** 157–82
- [19] Stekel D, Rashbass J and Williams E 1995 A computer graphic simulation of squamous epithelium *J. Theor. Biol.* **175** 283–93
- [20] Love A 1944 *A Treatise on the Mathematical Theory of Elasticity* (New York: Dover)
- [21] Wei C, Lintilhac P and Tanguay J 2001 An insight into cell elasticity and load bearing ability: measurement and theory *Plant Physiol.* **126** 1129–38
- [22] Chu Y-S, Dufour S, Thiery J, Perez E and Pincet F 2005 Johnson–Kendall–Roberts theory applied to living cells *Phys. Rev. Lett.* **94** 028102